nature COMMUNICATIONS

ARTICLE

Received 20 Sep 2012 | Accepted 19 Dec 2012 | Published 5 Feb 2013

DOI: 10.1038/ncomms2401

Spatial separation of photogenerated electrons and holes among {010} and {110} crystal facets of $BiVO_4$

Rengui Li[1,2,*], Fuxiang Zhang[1,*], Donge Wang[1], Jingxiu Yang[1,2], Mingrun Li[1], Jian Zhu[1,2], Xin Zhou[1], Hongxian Han[1] & Can Li[1]

Charge separation is crucial for increasing the activity of semiconductor-based photocatalysts, especially in water splitting reactions. Here we show, using monoclinic bismuth vanadate crystal as a model photocatalyst, that efficient charge separation can be achieved on different crystal facets, as evidenced by the reduction reaction with photogenerated electrons and oxidation reaction with photogenerated holes, which take place separately on the {010} and {110} facets under photo-irradiation. Based on this finding, the reduction and oxidation cocatalysts are selectively deposited on the {010} and {110} facets respectively, resulting in much higher activity in both photocatalytic and photoelectrocatalytic water oxidation reactions, compared with the photocatalyst with randomly distributed cocatalysts. These results show that the photogenrated electrons and holes can be separated between the different facets of semiconductor crystals. This finding may be useful in semiconductor physics and chemistry to construct highly efficient solar energy conversion systems.

[1] State Key Laboratory of Catalysis, Dalian Institute of Chemical Physics, Chinese Academy of Sciences, Dalian National Laboratory for Clean Energy, Zhongshan Road 457, Dalian 116023, China. [2] Graduate University of Chinese Academy of Sciences, Beijing 100049, China. *These authors contributed equally to this work. Correspondence and requests for materials should be addressed to C.L. (email: canli@dicp.ac.cn).

Charge separation has a key role in determining solar energy conversion efficiency of semiconductor-based systems for producing solar electricity and solar fuels through solar cells[1–4], photoelectrocatalysis[5–8] and photocatalysis[9–13]. As a key step in energy conversion, electron-hole pairs generated by light absorption need to be separated and transferred to the surface of the semiconductors[1,9,14–17]. Hence, an in-depth understanding of charge separation within semiconductors is desirable for the construction of an efficient solar energy conversion system.

Recent investigations on crystal facet engineering of semiconductors have demonstrated that photoexcited electrons and holes may be driven to different crystal facets. Thus, certain facets of a semiconductor prefer reduction while others favour oxidation[18–20]. However, reports on the reduction and oxidation reaction facets on the same semiconductor crystal (such as TiO_2) were often contradictory in the literature[21–26]. For example, it was reported that rutile {011} and anatase {001} faces provided the sites for oxidation, while the rutile {110} and anatase {101} faces offered the sites for reduction[24]. Similar phenomena were also reported in other references[27–29]. However, some references observed higher photocatalytic oxidation activity of organics on anatase nanocrystals with well-faceted {101} surfaces than that of the above-mentioned {001} facet[30–32]. Farneth *et al.*[21] concluded that the fine Ag particles are mostly deposited by reduction of Ag^+ on the {110} face of TiO_2, while Hotsenpiller *et al.*[22] reached the conclusion that the Ag particles were photocatalytically deposited at higher velocities on the {001} and {011} facets than on the {110} and {010} facets. A possible reason for the contrary conclusions is that the reaction selectivity on different facets is also affected by adsorption/desorption behaviours of reactant molecules and reaction intermediates on different facets[33,34]. A semiconductor with 1-D nanostructure and different crystal orientations has been proposed to lead to more efficient separation of electrons and holes with respect to the bulk material to explain the increased solar energy conversion efficiency[35–39], though experimental evidence on the separation of electrons and holes on different crystal facets remains elusive.

Here, we present experimental evidence for the separation of electrons and holes between the {010} and {110} crystal facets of the model semiconductor bismuth vanadate ($BiVO_4$). Facet-selective photo-deposition of metal ions, combined with promotion of water oxidation in photoelectrochemical and photocatalytic processes, clearly indicates the separation of electrons and holes to different facets. Meanwhile, various precursors of different metal ions as well as some distinct electron donors/acceptors were employed for the metal photo-deposition to rule out the adsorption effect.

Results

Selection of $BiVO_4$ as a model photocatalyst. $BiVO_4$, as a visible-light-responsive photocatalyst, has attracted increasing attention in photocatalytic[15,40–42] and photoelectrochemical[43–45] water oxidation. In addition, the $BiVO_4$ with large crystal size and controllable exposed facets can be easily prepared. Combined with advantages such as superior light absorbance, good photocatalytic activity, smooth exposed facets and non-toxic properties, $BiVO_4$ is chosen as an ideal model photocatalyst.

A large single crystal of monoclinic $BiVO_4$ was prepared by the hydrothermal method[46,47], and characterised by XRD patterns, UV–vis spectra and SEM images. The as-prepared $BiVO_4$ powder shows a smooth surface, regular decahedron shape, good crystallinity and characteristic visible-light absorption (Supplementary Fig. S1).

Facet-selective photo-deposition of metals/metal oxides. The photo-depositions of metals on the surface of $BiVO_4$ were carried out using $HAuCl_4$ (H_2PtCl_6 and $AgNO_3$) as precursors and water as a hole scavenger. SEM images (Fig. 1a–d) clearly show that the particles of Ag, Au and Pt (although with different particle sizes) are all solely deposited on the {010} facets. XPS spectra of Au 4f, Pt 4f and Ag 3d reveal that the deposited elements on the $BiVO_4$ are all in metallic form except that a small portion of incompletely reduced PtO species remained for the Pt/$BiVO_4$ sample (Supplementary Fig. S2). Decrease of the metal valence

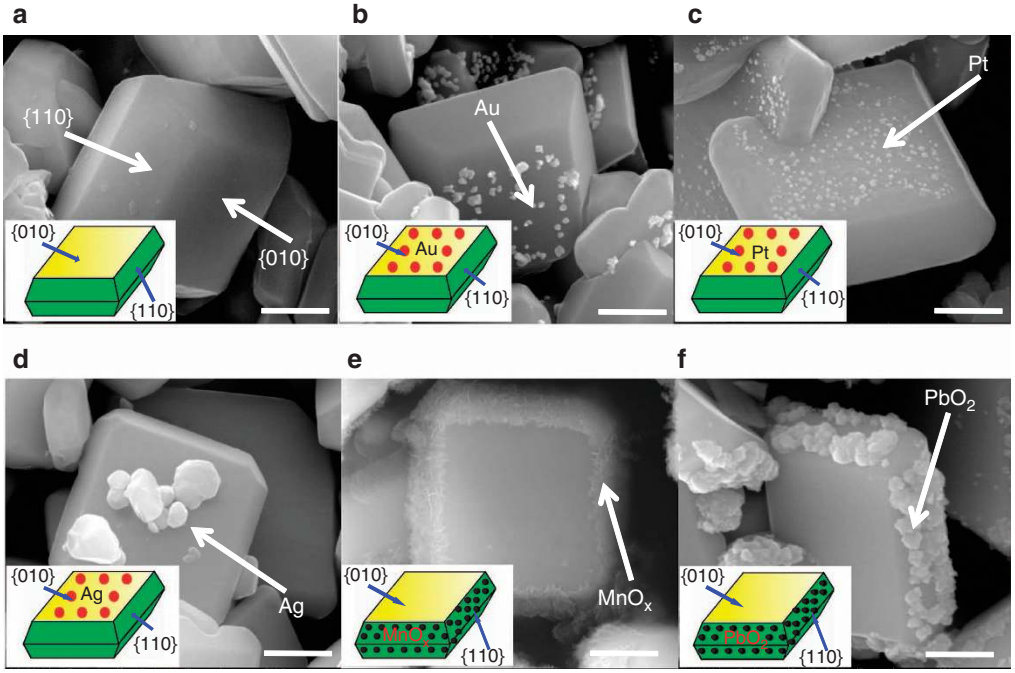

Figure 1 | SEM images of $BiVO_4$ with and without single metal/oxide deposited. (**a**) $BiVO_4$; (**b**) Au/$BiVO_4$; (**c**) Pt/$BiVO_4$; (**d**) Ag/$BiVO_4$; (**e**) MnO_x/$BiVO_4$ and (**f**) PbO_2/$BiVO_4$. The contents of the deposited metals/metal oxides are all 5 wt%. Scale bar, 500 nm.

with respect to the metal ion precursors indicates that the metal ions are photo-reduced on the {010} facets. Namely, the photo-generated electrons are readily available for the reduction reaction on the {010} facets. The photo-reduction of metal ions (equation 1) accompanying the elimination of photogenerated holes by water oxidation (equation 2) can be described as follows:

$$M^{n+} + ne^- \rightarrow M^0 \quad (1)$$

$$2H_2O + 4h^+ \rightarrow O_2 + 4H^+ \quad (2)$$

Photo-oxidation depositions of Mn^{2+} or Pb^{2+} ions on $BiVO_4$ were performed with IO_3^- as electron acceptors. Sponge-like manganese oxide deposits (Fig. 1e) and large lead oxide particles (Fig. 1f) are formed selectively on the {110} facets instead of the {010} facets. According to the binding energies of Pb 4f and Mn 2p in XPS (Supplementary Fig. S3), the deposited lead and manganese species can be ascribed to PbO_2 and MnO_x, respectively, where x is between 1.5 and 2.0 because the observed binding energies of manganese oxides are between those of Mn_2O_3 and MnO_2. High-resolution TEM images (Supplementary Fig. S4) show that the planar spaces of 2.715 Å and 1.663 Å well match the (222) and (440) planes of cubic Mn_2O_3, and the planar space of 1.663 Å is in accordance with the (102) plane of hexagonal MnO_2, further confirming the formation of MnO_x. The formation of PbO_2 and MnO_x oxides is an indication that the photo-oxidation selectively takes place on the {110} facets, that is, the photogenerated holes tend to migrate to the {110} facets for selective metal oxidation. The reactions can be summarised in equations (3) and (4):

$$M'^{m+} + xH_2O + (2x-m)h^+ \rightarrow M'O_x + 2xH^+ \quad (3)$$

$$IO_3^- + 6e^- \rightarrow I^- + \frac{3}{2}O_2 \quad (4)$$

Following the selective photo-deposition of single metals and metal oxides, we further investigated the photo-deposition of dual precursors with simultaneous reduction and oxidation reactions. The as-prepared samples are denoted as $Au/MnO_x/BiVO_4$, $Pt/MnO_x/BiVO_4$, $Ag/MnO_x/BiVO_4$, $Ag/PbO_2/BiVO_4$, $Au/PbO_2/BiVO_4$ and $Pt/PbO_2/BiVO_4$. It is interesting to note that the Au, Pt and Ag particles are still selectively photo-deposited on the {010} facets, while the MnO_x and PbO_2 particles are loaded only on the {110} facets of $BiVO_4$. This demonstrates that the facet-selective photo-deposition rules are also applied for the photo-deposition of dual components regardless of their combination order (Fig. 2). The selective photo-deposition of the precursors is not obviously affected by the experimental conditions, supporting the fact that the {110} and {010} facets prefer the oxidation and reduction reaction, respectively. The mechanisms of the above-mentioned photo-depositions are schematically described in Fig. 3, and the detailed experimental parameters are summarised in Supplementary Table S1. All these results unambiguously reveal that the photogenerated electrons and holes tend to accumulate on the {010} and {110} facets, respectively, which results in the reduction and oxidation reactions taking place on the corresponding {010} and {110} facets.

Water oxidation by photoelectrochemical process. In order to further illustrate the existence of the redox functional facets, the photoelectrochemical water oxidation of $BiVO_4$ with oxidation cocatalyst selectively deposited on different facets were examined. In this study, we prepared four typical photoanode electrodes denoted as $BiVO_4$, MnO_x (P.D.)/$BiVO_4$, MnO_x (imp)/$BiVO_4$ and IrO_2 (P.D.)/$BiVO_4$, respectively. To achieve different deposition morphologies of the cocatalysts, the MnO_x particles were deposited on the surface of $BiVO_4$ by two approaches. One is the selective photo-oxidation deposition introduced in this work (noted as MnO_x(P.D.)/$BiVO_4$), and the other is the impregnation method that normally results in random dispersion (noted as MnO_x(imp)/$BiVO_4$). Compared with the parent $BiVO_4$ electrode, the photoanode current in Fig. 4 is obviously increased when the oxidation cocatalyst MnO_x is selectively deposited on the {110} facets, while the randomly dispersed MnO_x on both {010} and

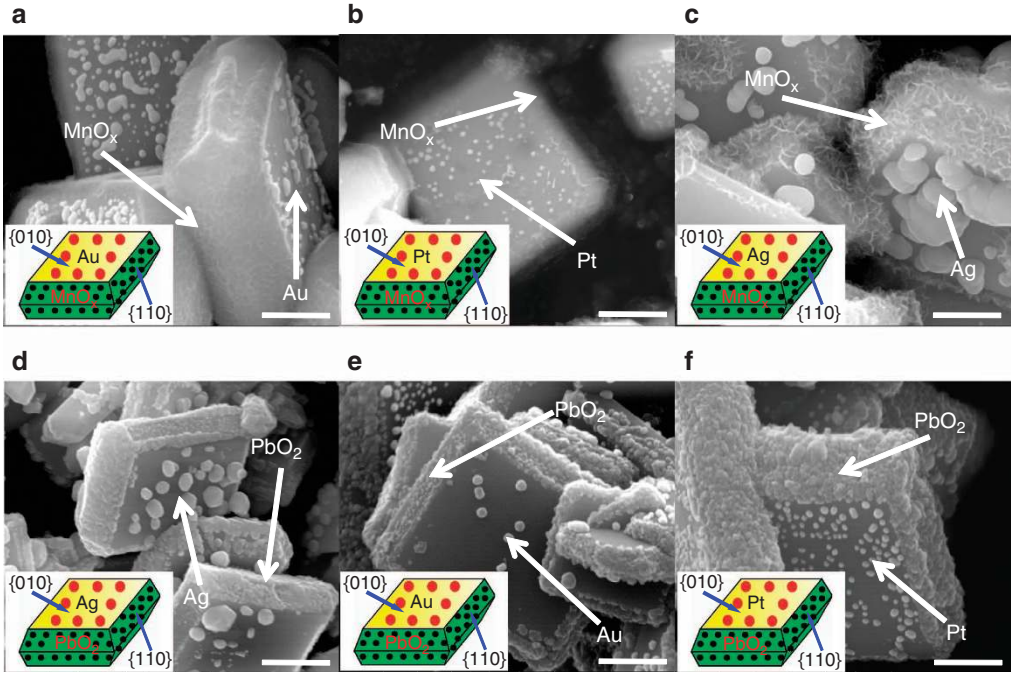

Figure 2 | SEM images of dual components photo-deposited on the surface of $BiVO_4$. (**a**) $Au/MnO_x/BiVO_4$, (**b**) $Pt/MnO_x/BiVO_4$, (**c**) $Ag/MnO_x/BiVO_4$, (**d**) $Ag/PbO_2/BiVO_4$, (**e**) $Au/PbO_2/BiVO_4$ and (**f**) $Pt/PbO_2/BiVO_4$. The contents of the deposited metals/metal oxides are all 5 wt %. Scale bar, 500 nm.

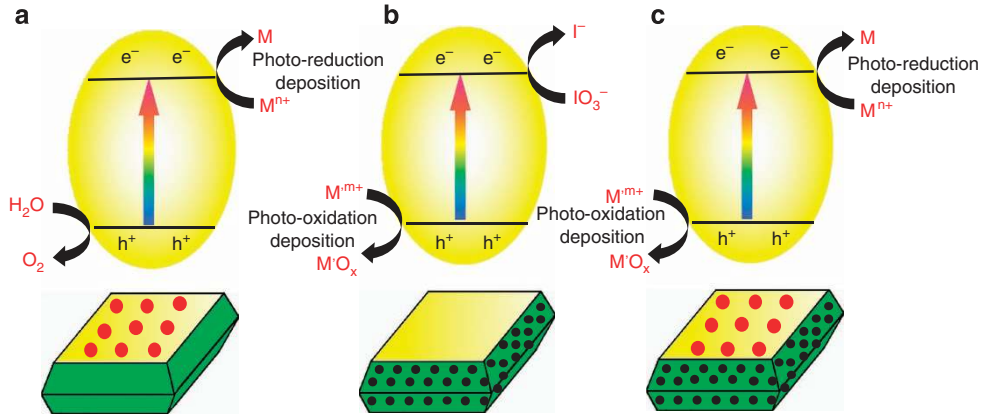

Figure 3 | Selective photo-deposition on $BiVO_4$. (**a**) photo-reduction deposition of noble metals on the {010} facet, (**b**) photo-oxidation deposition of metal oxides on the {110} facet and (**c**) simultaneous photo-deposition of metal and metal oxides on the {010} and {110} facets, respectively.

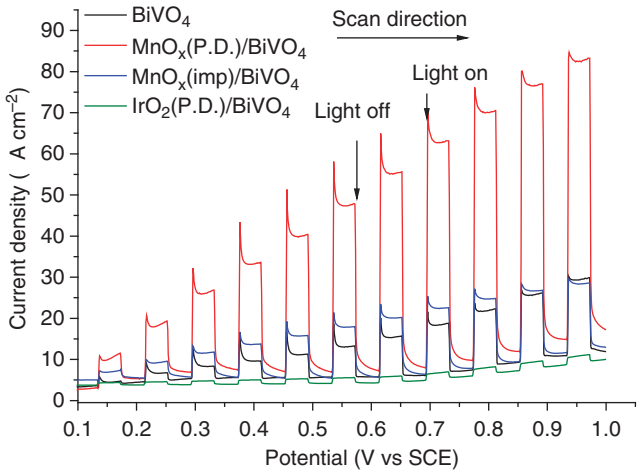

Figure 4 | Photochemical performances of four typical photoelectrodes. Black line: $BiVO_4$; red line: MnO_x (P.D.)/$BiVO_4$; blue line: MnO_x (imp)/$BiVO_4$; green line: IrO_2 (P.D.)/$BiVO_4$. P.D., photo-deposition, imp, impregnation. The MnO_x nanoparticles on the MnO_x (P.D.)/$BiVO_4$ are selectively deposited on the {110} facets, the MnO_x particles on the MnO_x (imp)/$BiVO_4$ photoelectrodes are randomly dispersed on both {110} and {010} facets, and the IrO_2 nanoparticles on the IrO_2 (P.D.)/$BiVO_4$ electrode was deposited selectively on the {010} facets. The contents of the deposited cocatalysts are all 0.1 wt %. Reaction conditions: 0.5 M Na_2SO_4 aqueous solution (pH = 6.8). Light source, 300 W Xe lamp ($\lambda \geq 420$ nm), Scan rate: 10 mV s^{-1}.

{110} facets results in a slightly enhanced photocurrent. This demonstrates the photocurrent can be efficiently promoted only when the hole-trapping oxidation cocatalyst is selectively deposited on the {110} facets. On the other hand, the IrO_2 particles were firstly deposited by selective photo-deposition of metallic Ir particles on the {010} facets and subsequent calcination in air to convert the metallic iridium particles into IrO_2. Decrease of photocurrent was observed for this sample with IrO_2 deposited on the {010} facets. This result indicates that if the cocatalysts deposited on the wrong facets, the photocurrent will be decreased. The typical SEM images (Supplementary Fig. S5) of the deposited oxides confirmed that the photo-deposited MnO_x and IrO_2 are selectively located on the {110} and {010} facets, respectively, while the MnO_x(imp) particles are randomly dispersed on all facets.

Water oxidation by photocatalysis. Photocatalytic water oxidation using a powder photocatalyst was also evaluated for the $BiVO_4$ samples modified with reduction or/and oxidation cocatalysts. The cocatalysts were deposited by two methods: one is the facet-selective photo-deposition employed in this work to realise the selective deposition on a specific facet, the other is impregnation method normally resulting in random dispersion of deposited cocatalysts on all facets of $BiVO_4$ (Supplementary Fig. S6). As shown in Fig. 5, the photocatalytic oxygen evolution activity is strongly dependent on the species of cocatalyst and the deposition methods. The highest water oxidation activity is achieved for the Pt(P.D.)/MnO_x(P.D.)/$BiVO_4$ sample with metallic platinum and MnO_x particles selectively photo-deposited on the {010} and {110} facets, respectively. It should be pointed out that the contents of the deposited MnO_x and Pt for photocatalytic water oxidation were all optimised to 0.1 wt% per ICP–AES analysis. The deposited metallic platinum on the {010} facets can collect electrons to reduce IO_3^- ions, and the MnO_x particles photo-deposited selectively on the {110} facets can accumulate holes for water oxidation. Although sizes of the deposited platinum particles are similarly in the range of 10 ~ 30 nm for the cocatalysts located by both photo-deposition and impregnation methods, the promotion effect of cocatalysts deposited by impregnation method is not as evident as that by the photo-deposition. This result indicates that when the reduction/oxidation cocatalysts are selectively deposited on the corresponding reduction/oxidation reaction facets, namely when the cocatalysts are on the right facets of $BiVO_4$, the photocatalytic performance can be most greatly enhanced.

Discussion

Photocatalytic reactions can usually be used to explore the reduction and oxidation sites of photocatalysts, because the photogenerated electrons just work for the photo-reduction reaction, while the photogenerated holes are only available for the photo-oxidation[48]. It is reasonable to deduce that if a crystal facet selectively accumulates electrons or holes, the facet will just work for reduction or oxidation separately. As a result, metals/oxides can be selectively deposited on the specific facets via photo-reduction or photo-oxidation reactions. On the other hand, if a certain crystal facet of a semiconductor equally traps both photogenerated electrons and holes, the photo-reduction and photo-oxidation reactions could proceed on the same crystal facet. In this case, the selective photo-deposition of metal ions on the facets would also occur due to the existence of two

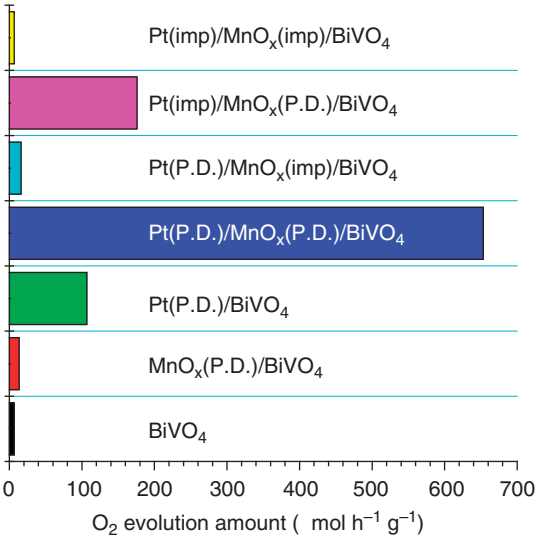

Figure 5 | Photocatalytic water oxidation performance of $BiVO_4$. Reaction conditions: 150 ml 0.02 M $NaIO_3$ aqueous solution, 300 W Xe lamp ($\lambda \geq 420$ nm), top irradiation, reaction time: 1 h. (imp, impregnation method; P.D., photo-deposition method; the contents of the deposited cocatalysts are all 0.1 wt%).

possibilities: one is the accumulation of electrons or holes on the facet, the other is the selective adsorption of the reactants on the given facet[34].

The possibility for preferential adsorption of anions or selective adsorption of metal ions, leading to selective photo-deposition, can be ruled out in this work because of the following experimental facts. On the one hand, various metal precursors ($AgNO_3$, $HAuCl_4$, H_2PtCl_6, $Pb(NO_3)_2$, $MnSO_4$) with different anionic species such as Cl^-, NO_3^- and SO_4^{2-} are employed, but the selective photo-deposition of metals and oxides are not changed. For example, the deposition of noble metals Au, Pt and Ag from precursors with distinct anions always selectively proceeded on the {010} facets of $BiVO_4$ photocatalyst. On the contrary, the deposition of Ag and PbO_2 on the {010} and {110} facets, respectively, are observed when the precursors with the same NO_3^- anions are applied. Moreover, the manganese ions are similarly deposited on the {110} facets (Supplementary Fig. S7) even though the precursors with distinct anions, such as Cl^-, SO_4^{2-} and NO_3^- and so on, are applied.

On the other hand, the isoelectric point of $BiVO_4$ was measured to be about 3.5, close to the values reported in the literature[49,50], which is slightly lower than the pH values of the photo-deposition solutions (Supplementary Table S1), indicating that the surfaces of $BiVO_4$ are negatively charged during the photo-deposition. As a consequence, the adsorption of $AuCl_4^-$ or $PtCl_6^{2-}$ anions on the surface of $BiVO_4$ should be less favourable than that of Ag^+, Pb^{2+} or Mn^{2+} cations in consideration of adsorption competition of ions with the same charge. However, the gold and platinum complex anions ($AuCl_4^-$, $PtCl_6^{2-}$) and silver cations (Ag^+) are all photo-reduced selectively on the {010} facets, while both the lead and manganese cations are photo-oxidised on the {110} facets. In addition, we also attempted to deposit noble Au, Pt and Ag by employing methanol instead of water as hole scavengers, and found that all of these metals are selectively deposited on the {010} facets of $BiVO_4$ (Supplementary Fig. S8). Therefore, the influence of adsorption on the selective photo-deposition behaviours caused by the pH environment, absorption of special ions and organic sacrificial reagent like methanol can also be ruled out.

Exclusion of the adsorption effect originating from the precursor ions and preparative environments renders us to reasonably ascribe the facet-selective photo-deposition of metals and oxides to the accumulation of electrons and holes on the {010} and {110} facets of $BiVO_4$, respectively, which correspondingly function as reduction and oxidation facets. It is reasonable to deduce that the accumulation of electrons and holes originates from charge separation on different facets. The origin of the charge separation on the {010} and {110} crystal facets of TiO_2 has been already estimated by theoretical calculation[19]. Similarly, we also evaluated the energy levels of {010} and {110} facets of $BiVO_4$ by DFT calculation method. A slight difference in energy of the valance and conduction band between {010} and {110} facets (Supplementary Fig. S9) suggests that the electron transfer from {110} to {010} facets is feasible thermodynamically, leading to the accumulation of electrons and holes separately on the {010} and {110} facets. It is worth noting that the band bending of each facet may be distinct due to their different surface electronic structures, as should be another factor affecting the spatial charge separation.

To further confirm the efficient charge separation on different crystal facets, the influence of temperature on the facet-selective photo-deposition was also examined (Supplementary Fig. S10). The morphology of the facet selectively deposited Au and MnO_x is independent of the temperature in the experimental conditions ($<100\,^{\circ}C$), except that the particle size of the deposited metals is slightly varied with increasing deposition temperature. The temperature-independent facet-selective metal deposition also indicates that the facet-selective deposition is not due to the selective adsorption effect which is usually temperature dependent.

The separation of the photogenerated electrons and holes on the {010} and {110} facets of $BiVO_4$ is further supported by our photoelectrochemical or photocatalystic water oxidation reaction. It has been known that if the oxidation cocatalyst is deposited on the oxidation sites of the photoelectrode, the photoanode currents can be increased because hole trapping on the oxidation cocatalyst can lead to better charge separation[51–55]. Indeed, our photoelectrochemical measurements show that the photoanode current was remarkably enhanced when the MnO_x was selectively photo-deposited on the hole-concentrated {110} facets of $BiVO_4$ (Fig. 3). In contrast, when the oxidation cocatalyst IrO_2 was controllably deposited on the electron-accumulated {010} facet, the performance of water oxidation is inhibited. Similarly, only when reduction cocatalyst Pt and oxidation cocatalyst MnO_x are selectively photo-deposited on the {010} and {110} facets of $BiVO_4$, the photocatalytic activity of water oxidation can be most greatly enhanced (Fig. 4). Based on these observations, we conclude that the photogenerated electrons and holes on the surface of $BiVO_4$ are accumulated on the {010} and {110} facets for reduction and oxidation reaction, respectively.

In summary, taking $BiVO_4$ as a model semiconductor, we confirm the existence of oxidation and reduction facets, which are evidenced by facet-selective photo-deposition of metals and oxides, and promotion of photocatalytic or photoelectrochemical water oxidation reaction by controllable deposition of the oxidation/reduction cocatalysts on the corresponding oxidation/reduction facets. The observation of the functional facets of the $BiVO_4$ crystal reveals spatial separation of the photogenerated electrons and holes between {010} and {110} facets of $BiVO_4$, which are mainly owing to the difference of energy levels of these facets. Our results also show the importance of the cocatalysts loading on the right crystal facets for efficient photocatalytic water splitting. The findings of functional redox facets, selective deposition of redox cocatalysts on the different facets of a single crystal, and efficient charge separation between different facets

should be promising and intriguing for understanding the mechanism of photocatalytic reactions, and designing highly efficient solar energy conversion photocatalysts/devices.

Methods

Facet-selective photo-deposition of metals and/or oxides. $BiVO_4$ sample was synthesised by a hydrothermal procedure (Supplementary Methods). For the facet-selective photo-depositions, three ways containing single reduction, single oxidation as well as simultaneous reduction and oxidation were carried out at room temperature without pH value adjusted. Normally, 0.50 g $BiVO_4$ powder and a calculated amount of metal precursors (5 wt%) were mixed in 100 ml deionised water. The suspension was then irradiated by a 300-W Xe lamp ($\lambda \geq 420$ nm) under continuous stirring. After 5 h photo-deposition, the suspension was filtered, washed with deionised water for more than three times, and finally dried at 60 °C for overnight. For comparison, the simultaneous photo-deposition of gold and manganese was also carried out at 50 and 90 °C, respectively. The as-obtained powder was used for characterizations and/or activity tests.

Preparation of photoelectrodes. The $BiVO_4$ film electrodes were prepared by electrophoretic deposition on FTO substrate ($1 \times 2\ cm^2$)[47], followed by drying in air and calcination at 573 K for 1 h. On the surface of the $BiVO_4$ electrode, different cocatalysts containing MnO_x or IrO_2 were subsequently deposited. As for the MnO_x deposition, two methods were employed for comparison. One is the {110} facet-selective photo-deposition method that was carried out in a Pyrex reactor in 0.01 M $MnSO_4$ solution containing 0.02 M $NaIO_3$, and illuminated from the top using a 300-W Xe lamp. The other is the conventional impregnation method, that is, impregnation of Mn $(NO_3)_2$ solutions (0.01 M) on the $BiVO_4$ electrode followed by calcination under 573 K for 1 h. The as-prepared electrodes are denoted as MnO_x(P.D.)/$BiVO_4$ and MnO_x(imp)/$BiVO_4$, respectively. The IrO_2(P.D.)/$BiVO_4$ electrode was prepared by selective photo-deposition of metallic iridium on the {010} facet of $BiVO_4$ from 1 mM Na_2IrCl_6 solution, which was transferred into IrO_2 by calcination in air at 573 K for 1 h.

Water oxidation by photoelectrochemical process. The Photoelectrochemical performances of the photoanodes were measured in a three-electrode setup, where Pt electrode and saturated mercury electrode were employed as counter and reference electrode, respectively. Electrolyte was 0.5 M Na_2SO_4 (pH = 6.8) solution. For linear sweep voltammetry, the potential was swept with scan rate of 10 mV s^{-1}. A shutter was used to record both the dark and photocurrent during a single scan. A 300-W Xe lamp (Ushio-CERMAXLX300) and optical cutoff filter (Kenko, L-42; $\lambda \geq 420$ nm) was used as light source. The contents of the deposited cocatalysts are all 0.1 wt% regardless of the methods, which were confirmed by ICP–AES analysis.

Water oxidation by photocatalysis. The photocatalytic O_2 evolution reactions were carried out in a closed gas circulation and evacuation system using a 300-W Xe lamp (Ushio-CERMAXLX300) and optical cutoff filter (Kenko, L-42; $\lambda \geq 420$ nm). Normally, 0.15 g photocatalyst was dispersed in 150 ml 0.02 M $NaIO_3$ aqueous solution in a Pyrex reaction cell. Before irradiation, the reaction system was thoroughly degassed by evacuation in order to drive off the air inside. The amount of evolved O_2 was determined by an online gas chromatograph (Agilent, GC-7890, TCD, Ar carrier). The rate of O_2 evolution in the initial 1 h was recorded for comparison. The contents of the deposited cocatalysts are all 0.1 wt% regardless of the methods, which were confirmed by ICP–AES analysis.

References

1. Ardo, S. & Meyer, G. J. Photodriven heterogeneous charge transfer with transition-metalcompounds anchored to TiO_2 semiconductor surfaces. *Chem. Soc. Rev.* **38,** 115–164 (2008).
2. Bakulin, A. A., Rao, A. & Pavelyev, V. G. *et al.* The role of driving energy and delocalized states for charge separation in organic semiconductors. *Science* **335,** 1340–1344 (2012).
3. Tisdale, W. A., Williams, K. & Timp, B. *et al.* Hot-electron transfer from semiconductor nanocrystals. *Science* **328,** 1543–1547 (2010).
4. Hagfeldt, A. & Grätzel, M. Molecular photovoltaics. *Acc. Chem. Res.* **33,** 269–277 (2000).
5. Hagfeldt, A., Björkstén, U. & Lindquist, S. E. Photoelectrochemical studies of colloidal TiO_2-films: the charge separation process studied by means of action spectra in the UV region. *Sol. Energy Mater. Sol. Cells* **27,** 293–304 (1992).
6. Higashimoto, S., Sakiyama, M. & Azuma, M. *et al.* Photoelectrochemical properties of hybrid WO_3/TiO_2 electrode. Effect of structures of WO_3 on charge separation behavior. *Thin Solid Films* **503,** 201–206 (2006).
7. Kavan, L., Grätzel, M. & Gilbert, S. *et al.* Electrochemical and photoelectrochemical investigation of single-crystal anatase. *J. Am. Chem. Soc.* **118,** 6716–6723 (1996).
8. Poznyak, S., Kokorin, A. & Kulak, A. *et al.* Effect of electron and hole acceptors on the photoelectrochemical behaviour of nanocrystalline microporous TiO_2 electrodes. *J. Electroanal. Chem.* **442,** 99–105 (1998).
9. Tachibana, Y., Vayssieres, L. & Durrant, J. Artificial photosynthesis for solar water-splitting. *Nat. Photon.* **6,** 511–518 (2012).
10. Chen, X., Shen, S. & Mao, S. S. *et al.* Semiconductor-based photocatalytic hydrogen generation. *Chem. Rev.* **110,** 6503 (2010).
11. Ariando *et al.* Electronic phase separation at the $LaAlO_3$/$SrTiO_3$ interface. *Nat. Commun.* **2,** 1–7 (2011).
12. Zhang, J., Xu, Q., Feng, Z., Li, M. & Li, C. Importance of the relationship between surface phases and photocatalytic activity of TiO_2. *Angew. Chem. Int. Ed.* **47,** 1766–1769 (2008).
13. Kim, H. G., Borse, P. H., Choi, W. & Lee, J. S. *et al.* Photocatalytic nanodiodes for visible-light photocatalysis. *Angew. Chem. Int. Ed.* **117,** 4661–4665 (2005).
14. Fujishima, A. *et al.* Electrochemical photolysis of water at a semiconductor electrode. *Nature* **238,** 37–38 (1972).
15. Kudo, A. & Miseki, Y. Heterogeneous photocatalyst materials for water splitting. *Chem. Soc. Rev.* **38,** 253–278 (2009).
16. Linsebigler, A. L. & Lu, G. Photocatalysis on TiO_2 surfaces: principles, mechanisms and selected results. *Chem. Rev.* **95,** 735–758 (1995).
17. McFarland, E. W. & Tang, J. A photovoltaic device structure based on internal electron emission. *Nature* **421,** 616–618 (2003).
18. Liu, G., Jimmy, C. Y. & Cheng, H. M. *et al.* Crystal facet engineering of semiconductor photocatalysts: motivations, advances and unique properties. *Chem. Commun.* **47,** 6763–6783 (2011).
19. Pan, J., Liu, G. & Cheng, H. M. *et al.* On the true photoreactivity order of {001},{010}, and {101} facets of anatase TiO_2 crystals. *Angew. Chem. Int. Ed.* **50,** 2133–2137 (2011).
20. Yang, H. G. *et al.* Anatase TiO_2 single crystals with a large percentage of reactive facets. *Nature* **453,** 638–641 (2008).
21. Farneth, W. E., McLean, R. S. & Barteau, M. A. *et al.* Tapping mode atomic force microscopy studies of the photoreduction of Ag^+ on individual submicrometer TiO_2 particles. *Langmuir* **15,** 8569–8573 (1999).
22. Hotsenpiller, P. A. M., Bolt, J. & Rohrer, G. *et al.* Orientation dependence of photochemical reactions on TiO_2 surfaces. *J. Phys. Chem. B* **102,** 3216–3226 (1998).
23. Lowekamp, J., Rohrer, G. & Farneth, W. *et al.* Anisotropic photochemical reactivity of bulk TiO_2 crystals. *J. Phys. Chem. B* **102,** 7323–7327 (1998).
24. Ohno, T., Sarukawa, K. & Matsumura, M. *et al.* Crystal faces of rutile and anatase TiO_2 particles and their roles in photocatalytic reactions. *New J. Chem.* **26,** 1167–1170 (2002).
25. Oliver, P. M., Watson, G. W. & Parker, S. C. *et al.* Atomistic simulation of the surface structure of the TiO_2 polymorphs rutileand anatase. *J. Mater. Chem.* **7,** 563–568 (1997).
26. Tachikawa, T., Yamashita, S. & Majima, T. *et al.* Evidence for crystal-face-dependent TiO_2 photocatalysis from single-molecule imaging and kinetic analysis. *J. Am. Chem. Soc.* **133,** 7197–7204 (2011).
27. Selloni, A. Crystal growth: anatase shows its reactive side. *Nat. Mater.* **7,** 613–615 (2008).
28. Zhu, J., Yang, H. & Li, H. *et al.* Solvothermally controllable synthesis of anatase TiO_2 nanocrystals with dominant {001} facets and enhanced photocatalytic activity. *Cryst. Eng. Comm.* **12,** 2219–2224 (2010).
29. Yang, X., Li, Z. & Li, C. *et al.* Ultra-thin anatase TiO_2 nanosheets dominated with {001} facets: thickness-controlled synthesis, growth mechanism and water-splitting properties. *Cryst. Eng. Comm.* **13,** 1378–1383 (2011).
30. Wu, N., Wang, J. & Manivannan, A. *et al.* Shape-enhanced photocatalytic activity of single-crystalline anatase TiO_2 (101) nanobelts. *J. Am. Chem. Soc.* **132,** 6679–6685 (2010).
31. Murakami, N., Tsubota, T. & Ohno, T. *et al.* Shape-controlled anatase titanium (IV) oxide particles prepared by hydrothermal treatment of Peroxo titanic acid in the presence of polyvinyl alcohol. *J. Phys. Chem. C* **113,** 3062–3069 (2009).
32. Cho, C. H., Han, M. H. & Kim, D. K. *et al.* Morphology evolution of anatase TiO_2 nanocrystals under a hydrothermal condition (pH = 9.5) and their ultra-high photo-catalytic activity. *Mater. Chem. Phys.* **92,** 104–111 (2005).
33. Miseki, Y., Kato, H. & Kudo, A. *et al.* Water splitting into H_2 and O_2 over niobate and titanate photocatalysts with (111) plane-type layered perovskite structure. *Energy Environ. Sci.* **2,** 306–314 (2009).
34. Read, C. G., Steinmiller, E. M. P. & Choi, K. S. *et al.* Atomic plane-selective deposition of gold nanoparticles on metal oxide crystals exploiting preferential adsorption of additives. *J. Am. Chem. Soc.* **131,** 12040–12041 (2009).
35. Wang, Z. & Song, J. Piezoelectric nanogenerators based on zinc oxide nanowire arrays. *Science* **312,** 242–246 (2006).
36. Jennings, J. R., Ghicov, A. & Walker, A. B. *et al.* Dye-sensitized solar cells based on oriented TiO_2 nanotube arrays: transport, trapping, and transfer of electrons. *J. Am. Chem. Soc.* **130,** 13364–13372 (2008).
37. Kumar, S., Jones, M. & Scholes, G. D. *et al.* Nanorod heterostructures showing photoinduced charge separation. *Small* **3,** 1633–1639 (2007).
38. Mor, G. K., Shankar, K. & Grimes, C. A. *et al.* Use of highly-ordered TiO_2 nanotube arrays in dye-sensitized solar cells. *Nano Lett.* **6,** 215–218 (2006).

39. Wu, K., Zhu, H. & Lian, T. *et al.* Ultrafast charge separation and long-lived charge separated state in photocatalytic CdS-Pt nanorod heterostructures. *J. Am. Chem. Soc.* **134,** 10337–10340 (2012).
40. Kudo, A., Omori, K. & Kato, H. *et al.* A novel aqueous process for preparation of crystal form-controlled and highly crystalline $BiVO_4$ powder from layered vanadates at room temperature and its photocatalytic and photophysical properties. *J. Am. Chem. Soc.* **121,** 11459–11467 (1999).
41. Kudo, A., Ueda, K. & Mikami, I. *et al.* Photocatalytic O_2 evolution under visible light irradiation on $BiVO_4$ in aqueous $AgNO_3$ solution. *Catal. Lett.* **53,** 229–230 (1998).
42. Xi, G. & Ye, J. Synthesis of bismuth vanadate nanoplates with exposed {001} facets and enhanced visible-light photocatalytic properties. *Chem. Commun.* **46,** 1893–1895 (2010).
43. Jo, W. J. *et al.* Phosphate doping into monoclinic $BiVO_4$ for enhanced photoelectrochemical water oxidation activity. *Angew. Chem. Int. Ed.* **51,** 3147–3152 (2012).
44. Ng, Y. H., Kudo, A. & Amal, R. *et al.* Reducing graphene oxide on a visible-light $BiVO_4$ photocatalyst for an enhanced photoelectrochemical water splitting. *J. Phys. Chem. Lett.* **1,** 2607–2612 (2010).
45. Sayama, K. *et al.* Photoelectrochemical decomposition of water into H_2 and O_2 on porous $BiVO_4$ thin-film electrodes under visible light and significant effect of Ag ion treatment. *J. Phys. Chem. B* **110,** 11352–11360 (2006).
46. Wang, D. *et al.* Crystal facet dependence of water oxidation on $BiVO_4$ sheets under visible light irradiation. *Chem. Eur. J.* **17,** 1275–1282 (2011).
47. Wang, D. *et al.* Photocatalytic Water oxidation on $BiVO_4$ with the electrocatalyst as an oxidation co-catalyst: essential relations between electrocatalyst and photocatalyst. *J. Phys. Chem. C* **116,** 5082–5089 (2012).
48. Kraeutler, B. & Bard, A. J. Heterogeneous photocatalytic preparation of supported catalysts. Photodeposition of platinum on titanium dioxide powder and other substrates. *J. Am. Chem. Soc.* **100,** 4317–4318 (1978).
49. Castillo, N. C., Ding, L. & Pulgarin, C. *et al.* On the photocatalytic degradation of phenol and dichloroacetate by $BiVO_4$: the need of a sacrificial electron acceptor. *J. Photochem. Photobiol. A* **216,** 221–227 (2010).
50. Zhou, B., Zhao, X. & Huang, C. *et al.* Visible-light sensitive cobalt-doped $BiVO_4$(Co-$BiVO_4$) photocatalytic composites for the degradation of methylene blue dye in dilute aqueous solutions. *Appl. Catal. B Environ.* **99,** 214–221 (2010).
51. Allongue, P., Blonkowski, S. & Souteyrand, E. Experimental investigation of charge transfer at the semiconductor/electrolyte junction. *Electrochim. Acta* **37,** 781–797 (1992).
52. Bach, U. *et al.* Solid-state dye-sensitized mesoporous TiO_2 solar cells with high photon-to-electron conversion efficiencies. *Nature* **395,** 583–585 (1998).
53. Hill, J. C. & Choi, K. S. Effect of electrolytes on the selectivity and stability of n-type WO_3 photoelectrodes for use in solar water oxidation. *J. Phys. Chem. C* **116,** 7612–7620 (2012).
54. Maeda, K., Higashi, M. & Domen, K. *et al.* $SrNbO_2N$ as a water-splitting photoanode with a wide visible light absorption band. *J. Am. Chem. Soc.* **133,** 12334–12337 (2011).
55. Wang, Y. *et al.* Photoelectrochemical properties of metal-ion-doped TiO_2 nanocrystalline electrodes. *Thin Solid Films* **349,** 120–125 (1999).

Acknowledgements

This work was financially supported by National Natural Science Foundation of China (No. 21061140361, 21090340); Solar Energy Action Plan of Chinese Academy of Sciences (ACS); Hundred Talents Programme of DICP, ACS; SKLC Independent Research Projects and 973 National Basic Research Programme of the Ministry of Science and Technology (Grant 2009CB220010).

Author contributions

C.L. and R.L. designed the experiments, R.L. performed the photo-deposition, water oxidation and most of characterizations, D.W. synthesized the $BiVO_4$, J.Y. and X.Z. carried out theoretical estimations. M.L. performed HR-TEM experiment. C.L., F.Z. and R.L. together wrote and revised the manuscript. H.H. took part in the revision of the manuscript. All authors discussed the results and commented on the manuscript.

Additional information

Supplementary Information accompanies this paper at http://www.nature.com/naturecommunications.

Competing financial interests: The authors declare no competing financial interests.

Reprints and permission information is available online at http://npg.nature.com/reprintsandpermissions.

How to cite this article: Li, R. *et al.* Spatial Separation of Photogenerated Electrons and Holes among {010} and {110} Crystal Facets of $BiVO_4$. *Nat. Commun.* 4:1432 doi: 10.1038/ncomms2401 (2013).